

# Kitaev interactions between $j=1/2$ moments in honeycomb $\text{Na}_2\text{IrO}_3$ are large and ferromagnetic: insights from *ab initio* quantum chemistry calculations

Vamshi M. Katukuri<sup>1</sup>, S. Nishimoto<sup>1</sup>, V. Yushankhai<sup>2,3</sup>,  
A. Stoyanova<sup>3</sup>, H. Kandpal<sup>1</sup>, Sungkyun Choi<sup>4</sup>, R. Coldea<sup>4</sup>,  
I. Rousochatzakis<sup>1</sup>, L. Hozoi<sup>1</sup> and Jeroen van den Brink<sup>1,5</sup>

<sup>1</sup>Institute for Theoretical Solid State Physics, IFW Dresden, Helmholtzstr. 20, 01069 Dresden, Germany

<sup>2</sup>Joint Institute for Nuclear Research, Joliot-Curie 6, 141980 Dubna, Russia

<sup>3</sup>Max-Planck-Institut für Physik komplexer Systeme, Nöthnitzer Str. 38, 01187 Dresden, Germany

<sup>4</sup>Clarendon Laboratory, University of Oxford, Parks Road, Oxford OX1 3PU, United Kingdom

<sup>5</sup>Department of Physics, Technical University Dresden, Helmholtzstr. 10, 01069 Dresden, Germany

E-mail: v.m.katukuri@ifw-dresden.de, s.nishimoto@ifw-dresden.de,  
l.hozoi@ifw-dresden.de, j.van.den.brink@ifw-dresden.de

**Abstract.**  $\text{Na}_2\text{IrO}_3$ , a honeycomb  $5d^5$  oxide, has been recently identified as a potential realization of the Kitaev spin lattice. The basic feature of this spin model is that for each of the three metal-metal links emerging out of a metal site, the Kitaev interaction connects only spin components perpendicular to the plaquette defined by the magnetic ions and two bridging ligands. The fact that reciprocally orthogonal spin components are coupled along the three different links leads to strong frustration effects and nontrivial physics. While the experiments indicate zigzag antiferromagnetic order in  $\text{Na}_2\text{IrO}_3$ , the signs and relative strengths of the Kitaev and Heisenberg interactions are still under debate. Herein we report results of *ab initio* many-body electronic-structure calculations and establish that the nearest-neighbor exchange is strongly anisotropic with a dominant ferromagnetic Kitaev part, whereas the Heisenberg contribution is significantly weaker and antiferromagnetic. The calculations further reveal a strong sensitivity to tiny structural details such as the bond angles. In addition to the large spin-orbit interactions, this strong dependence on distortions of the  $\text{Ir}_2\text{O}_2$  plaquettes singles out the honeycomb  $5d^5$  oxides as a new playground for the realization of unconventional magnetic ground states and excitations in extended systems.

## 1. Introduction

The Heisenberg model of magnetic interactions,  $J\mathbf{S}_i \cdot \mathbf{S}_j$  between spin moments at sites  $\{i, j\}$ , has been successfully used as an effective minimal model to describe the cooperative magnetic properties of both molecular and solid-state many-electron systems. A less conventional spin model – the Kitaev model [1] – has been recently proposed for honeycomb-lattice materials with  $90^\circ$  metal-oxygen-metal bonds and strong spin-orbit interactions [2]. It has nontrivial topological phases with elementary excitations exhibiting Majorana statistics, which are relevant and much studied in the context of topological quantum computing [1, 3, 4, 5, 6, 7]. Candidate materials proposed to host such physics are the honeycomb oxides  $\text{Na}_2\text{IrO}_3$  and  $\text{Li}_2\text{IrO}_3$  [2]. The magnetically active sites, the  $\text{Ir}^{4+}$  species, display in these compounds a  $5d^5$  valence electron configuration, octahedral ligand coordination and bonding of nearest-neighbor (NN) Ir ions through two ligands [8, 9]. In the simplest approximation, i.e., for sufficiently large  $t_{2g-e_g}$  octahedral crystal-field splittings within the Ir  $5d$  shell and degenerate Ir  $t_{2g}$  levels, the ground-state electron configuration at each Ir site is a  $t_{2g}^5$  effective  $j = 1/2$  spin-orbit doublet [10, 11, 12, 2]. The anisotropic, Kitaev type coupling then stems from the particular form the superexchange between the Ir  $j = 1/2$  pseudospins takes for  $90^\circ$  bond angles on the Ir-O<sub>2</sub>-Ir plaquette [2, 13, 14].

Recent measurements on  $\text{Na}_2\text{IrO}_3$  [8, 9] indicate significant lattice distortions away from the idealized case of cubic  $\text{IrO}_6$  octahedra and  $90^\circ$  Ir-O-Ir bond angles for which the Kitaev-Heisenberg (KH) model was proposed [2, 13]. Lower-symmetry crystal fields and distortions of the Ir-O-Ir bonds obviously give rise to finite Ir  $t_{2g}$  splittings [15, 16] and more complex superexchange physics [17, 18]. It has been actually shown that the interplay between “local” distortions of the O cage and longer-range crystal anisotropy is a key feature in  $5d$  oxides [19, 20, 21, 22, 23] and the outcome of this competition is directly related to the precise nature of the magnetic ground state [23]. Moreover, the lower symmetry characterizing a given  $[\text{Ir}_2\text{O}_{10}]$  unit of two edge-sharing octahedra allows in principle for nonzero anisotropic interaction terms beyond the Kitaev picture.

The inelastic neutron scattering data [8] and the magnetic ordering pattern [9, 24] in  $\text{Na}_2\text{IrO}_3$  could in principle be explained in a minimal model by either i) a more conventional Heisenberg model with frustrated exchange couplings extending up to third NN’s [8] or ii) a KH model with dominant antiferromagnetic (AF) Kitaev and smaller ferromagnetic (FM) Heisenberg NN terms [14]. The presence of strong Kitaev interactions has furthermore been suggested on the basis of recent resonant inelastic x-ray scattering experiments [25].

To clarify the signs and the strengths of the effective coupling constants in  $\text{Na}_2\text{IrO}_3$ , we here employ many-body *ab initio* techniques from wave-function-based quantum chemistry [26]. We establish that the situation is much more subtle than presumed so far. In model systems the KH Hamiltonian arises due to the destructive interference of different superexchange pathways that contribute equally to the effective intersite interaction [2, 13]. This interference turns out to be rather fragile as even when

we consider idealized structures with cubic  $\text{IrO}_6$  octahedra, orthogonal Ir-O-Ir bonds and  $D_{2h}$  point-group symmetry of the Ir-Ir link, the computed low-energy magnetic spectrum does not support a pure KH model. A careful analysis shows that in the Kitaev reference frame [2, 13] off-diagonal terms of the symmetric anisotropic exchange-coupling tensor are allowed by symmetry to be non-zero. The quantum chemistry (QC) calculations predict the latter are comparable in magnitude to the strength of the isotropic Heisenberg term. We find that the effective Kitaev coupling is, however, the dominant energy scale – depending on geometrical details in the range of 10–20 meV and FM – and that the NN Heisenberg  $J$  is AF and significantly weaker. For NN interaction parameters as derived in the QC study, we have further performed exact diagonalization (ED) calculations including additionally finite AF second and third order Ir-Ir Heisenberg couplings. These indicate the presence of zigzag AF order, in agreement with the experimentally observed spin texture [8, 9, 24].

## 2. Results and discussion

Multiconfiguration complete-active-space self-consistent-field (CASSCF) and multireference configuration-interaction (MRCI) calculations [26] were performed on embedded clusters made of two reference  $\text{IrO}_6$  octahedra (for technical details, see Appendix A). All possible occupations were allowed within the set of  $t_{2g}$  orbitals at the two magnetically active Ir sites in the CASSCF calculations. The orbitals were optimized for an average of the lowest nine singlets and the nine triplet states. All these singlet and

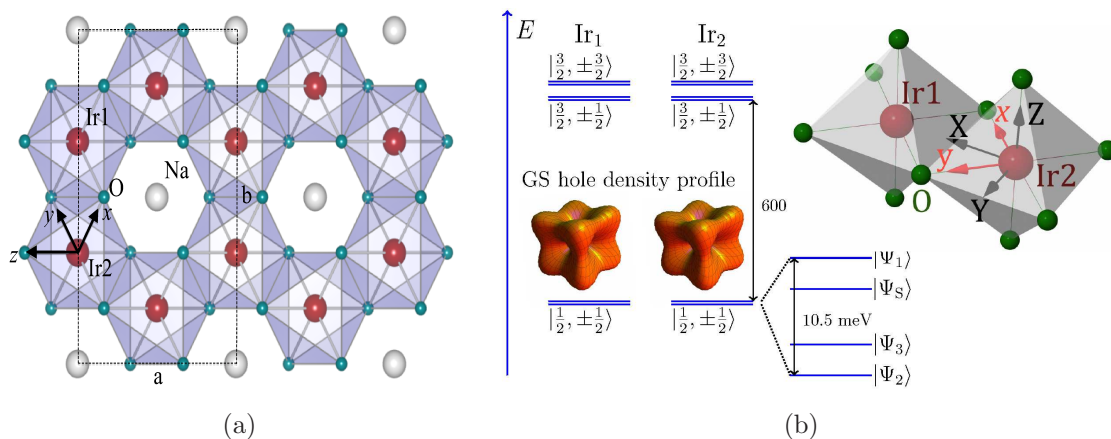


**Figure 1.** a) Ir honeycomb layer in  $\text{Na}_2\text{IrO}_3$ , idealized model with cubic  $\text{IrO}_6$  and  $\text{NaO}_6$  octahedra of equal size and  $90^\circ$  Ir-O-Ir bonds. b) Low-lying energy levels for two NN octahedra and ground-state (GS) density profiles for the effective spin-orbit  $j = 1/2$  states at each Ir site. The  $d$ -level splittings are not to scale, notations as in Table 1. The  $(x, y, z)$  coordinate frame used to express the KH Hamiltonian [2] is also drawn for one of the Ir-Ir links. For each  $\text{Ir}_2\text{O}_2$  plaquette in the actual  $C2/m$  structure [8], due to trigonal squashing of the  $\text{IrO}_6$  octahedra (normal to the Ir honeycomb plane), the apical-like Ir-O bonds are not along the corresponding Kitaev axis.

**Table 1.** Energy splittings of the four lowest magnetic states and effective coupling parameters (meV) for two NN  $\text{IrO}_6$  octahedra in the  $C2/m$  structure of Ref. [8]. The weight of  $(\uparrow\downarrow + \downarrow\uparrow)/\sqrt{2}$  and  $(\uparrow\uparrow + \downarrow\downarrow)/\sqrt{2}$  in  $\Psi'_1$  and  $\Psi'_2$ , respectively, is  $\approx 98\%$ , see text.

Method	CAS+SOC	MRCI+SOC
$\angle(\text{Ir-O-Ir})=90^\circ$ :		
$\Psi_S = (\uparrow\downarrow - \downarrow\uparrow)/\sqrt{2}$	0.0	0.0
$\Psi_2 = (\uparrow\uparrow + \downarrow\downarrow)/\sqrt{2}$	0.7	0.4
$\Psi_3 = (\uparrow\uparrow - \downarrow\downarrow)/\sqrt{2}$	0.7	1.1
$\Psi_1 = (\uparrow\downarrow + \downarrow\uparrow)/\sqrt{2}$	1.0	1.1
$(J,K,D)$	(1.0, -0.6, 0.0)	(1.1, -0.7, -0.7)
$\angle(\text{Ir-O-Ir})=98.5^\circ$ :		
$\Psi_2 = (\uparrow\uparrow + \downarrow\downarrow)/\sqrt{2}$	0.0	0.0
$\Psi_3 = (\uparrow\uparrow - \downarrow\downarrow)/\sqrt{2}$	1.2	2.1
$\Psi_S = (\uparrow\downarrow - \downarrow\uparrow)/\sqrt{2}$	4.3	5.1
$\Psi_1 = (\uparrow\downarrow + \downarrow\uparrow)/\sqrt{2}$	3.9	6.5
$(J,K,D)$	(-0.4, -6.6, -1.2)	(1.4, -10.9, -2.1)

triplet states entered the spin-orbit calculations, both at the CASSCF and MRCI levels. In MRCI, single and double excitations from the Ir  $t_{2g}$  shells and the  $2p$  orbitals of the bridging ligands were accounted for. A similar strategy of explicitly dealing only with selected groups of localized ligand orbitals was earlier adopted in QC studies on both  $3d$  [27, 28, 29, 30] and  $5d$  [20, 21, 23] compounds, with results in good agreement with the experiment [20, 21, 27, 28, 29, 30].

For a pair  $\{i, j\}$  of magnetic sites in systems in which the midpoint of the  $ij$  link displays inversion symmetry, the most general bilinear exchange Hamiltonian is

$$\mathcal{H}_{ij} = J_0 \tilde{\mathbf{S}}_i \cdot \tilde{\mathbf{S}}_j + \sum_{\alpha, \beta \in \{X, Y, Z\}} \Gamma_{\alpha\beta} \tilde{S}_i^\alpha \tilde{S}_j^\beta, \quad (1)$$

where  $\tilde{\mathbf{S}}_i, \tilde{\mathbf{S}}_j$  are pseudospin operators ( $\tilde{S} = 1/2$ ) [2, 13] and the elements  $\Gamma_{\alpha\beta}$  form a traceless symmetric second-rank tensor. It is convenient to choose the  $X$  axis along the Ir-Ir link and  $Z$  perpendicular to the plaquette defined by the two Ir ions and the two bridging ligands because in the  $C2/m$  crystal structure of  $\text{Na}_2\text{IrO}_3$ , for Ir-Ir bonds along  $b$ , see Fig. 1, the Ir-Ir axis is a  $C_2$  axis with an orthogonal mirror plane [8, 9], i.e., the symmetry of those  $[\text{Ir}_2\text{O}_{10}]$  units is  $C_{2h}$ . With such a choice of the coordinate system only  $\Gamma_{YZ} = \Gamma_{ZY}$  are finite and so

$$\Gamma = \begin{pmatrix} A & 0 & 0 \\ 0 & B & C \\ 0 & C & -A - B \end{pmatrix}_{\{X, Y, Z\}}. \quad (2)$$

The fact that  $Y$  and  $Z$  are not  $C_2$  axes is related to the configuration of the four adjacent Ir sites – two of those are below and two above the  $XY$  plane, with no inversion center – and the trigonal squashing of the  $\text{IrO}_6$  octahedra [8]. The KH Hamiltonian is however

expressed in a  $(x, y, z)$  coordinate frame that has the  $(x, y)$  coordinates rotated by  $45^\circ$  about the  $Z = z$  axis [2, 13], as compared to  $(X, Y)$ , see Fig. 1, and  $\Gamma$  then becomes

$$\Gamma = \begin{pmatrix} (A+B)/2 & (A-B)/2 & -C/\sqrt{2} \\ (A-B)/2 & (A+B)/2 & C/\sqrt{2} \\ -C/\sqrt{2} & C/\sqrt{2} & -A-B \end{pmatrix}_{\{x,y,z\}} \quad (3)$$

(see Appendix B for details).

For a more transparent picture and better insight into the nature of the NN magnetic couplings, it is instructive to first consider two-octahedra clusters taken from an idealized crystalline model without trigonal distortions and with all adjacent Ir and Na sites modeled as identical point charges. In this case, the overall symmetry is  $D_{2h}$  and *all* off-diagonal couplings cancel by symmetry, in the  $(X, Y, Z)$  coordinate system with  $X$  along the Ir-Ir link. For an idealized  $[\text{Ir}_2\text{O}_{10}]$  unit displaying  $D_{2h}$  symmetry  $C = 0$  and the spin Hamiltonian reduces to

$$\mathcal{H}_{ij}^{D_{2h}} = J \tilde{\mathbf{S}}_i \cdot \tilde{\mathbf{S}}_j + K \tilde{S}_i^z \tilde{S}_j^z + D \left( \tilde{S}_i^x \tilde{S}_j^y + \tilde{S}_i^y \tilde{S}_j^x \right), \quad (4)$$

where  $K = -\frac{3}{2}(A+B)$ ,  $J = J_0 - K/3$  and  $D = \frac{1}{2}(A-B)$ . The off-diagonal  $xy$  coupling, last term in (4), is allowed by symmetry even for ideal octahedra at  $90^\circ$  Ir-O-Ir bonding but has been neglected in earlier studies on  $\text{Na}_2\text{IrO}_3$  [2, 13, 14, 31, 16].

Results of spin-orbit calculations, both at the CASSCF (CAS+SOC) and MRCI (MRCI+SOC) levels, are listed for idealized  $[\text{Ir}_2\text{O}_{10}]$   $D_{2h}$  model clusters in Table 1. Such a cluster is highly charged, 12-. To ensure charge neutrality, we assigned to each of the 26 adjacent Na and Ir sites fictitious point charges of  $+12/26$ . In the simplest approximation, no farther embedding was used for these  $D_{2h}$  clusters. The *ab initio* calculations were performed for both i) regular  $\text{IrO}_6$  octahedra and  $90^\circ$  Ir-O-Ir bond angles and ii) distorted geometries with all ligands in the  $xy$  plane pushed closer to the Ir-Ir axis and therefore larger Ir-O-Ir bond angles but keeping the  $D_{2h}$  bond symmetry. The Ir-Ir distance  $d(\text{Ir-Ir})$  and in the latter case the Ir-O-Ir angle were set to 3.133 Å and  $98.5^\circ$ , respectively, average values in the  $C2/m$  crystal structure reported in [8].

To determine the nature of each spin-orbit state we explicitly compute the dipole and quadrupole transition matrix elements among those four low-lying states describing the magnetic spectrum of two edge-sharing octahedra. A careful symmetry analysis reveals that the spin-orbit wave functions  $\Psi_S, \Psi_1, \Psi_2$  and  $\Psi_3$  defined in Table 1 transform according to the  $A_g, B_{2u}, B_{1u}$  and  $A_u$  irreducible representations, respectively. Standard selection rules and the nonzero dipole and quadrupole matrix elements in the QC outputs then clearly indicate which state is which. We also carried out the transformation of the spin-orbit wave functions from the usual  $\{L_1, M_{L_1}, L_2, M_{L_2}, S, M_S\}$  basis in standard QC programs to the  $\{\tilde{S}_1, \tilde{S}_2, \tilde{M}_{S_1}, \tilde{M}_{S_2}\}$  basis. This allows the study of  $\Psi_1$ - $\Psi_2$  mixing when the point-group symmetry is reduced to  $C_{2h}$ , see below. Having the assignment of the states resolved, the  $\Psi_S$ - $\Psi_1$  splitting provides  $J$ , the  $\Psi_2$ - $\Psi_3$  splitting yields  $D$ , while the difference between the energy of  $\Psi_1$  and the average of the  $E_2(\Psi_2)$  and  $E_3(\Psi_3)$  eigenvalues equals  $-K/2$ , see Appendix A.

**Table 2.** Energy splittings of the four lowest magnetic states and effective coupling parameters (meV) for two NN  $\text{IrO}_6$  octahedra in the  $C2/m$  structure of Ref. [8]. The weight of  $(\uparrow\downarrow + \downarrow\uparrow)/\sqrt{2}$  and  $(\uparrow\uparrow + \downarrow\downarrow)/\sqrt{2}$  in  $\Psi'_1$  and  $\Psi'_2$ , respectively, is  $\approx 98\%$ , see text.

Method	CAS+SOC	MRCI+SOC
$\angle(\text{Ir-O-Ir})=99.45^\circ$ , $d(\text{Ir}_1\text{-Ir}_2)=3.138 \text{ \AA}$ ( $\times 1$ ) <sup>a</sup> :		
$\Psi'_2$	0.0	0.0
$\Psi_3 = (\uparrow\uparrow - \downarrow\downarrow)/\sqrt{2}$	0.2	0.5
$\Psi_S = (\uparrow\downarrow - \downarrow\uparrow)/\sqrt{2}$	4.4	5.5
$\Psi'_1$	6.3	10.5
$(J, K, D)$	(1.9, -12.4, -0.2)	(5.0, -20.5, -0.5)
$\angle(\text{Ir-O-Ir})=97.97^\circ$ , $d(\text{Ir}_2\text{-Ir}_3)=3.130 \text{ \AA}$ ( $\times 2$ ) <sup>b</sup> :		
$\Psi'_2$	0.0	0.0
$\Psi_3 = (\uparrow\uparrow - \downarrow\downarrow)/\sqrt{2}$	0.3	1.2
$\Psi_S = (\uparrow\downarrow - \downarrow\uparrow)/\sqrt{2}$	4.6	6.7
$\Psi'_1$	5.8	8.2
$(J, K, D)$	(1.2, -11.3, -0.3)	(1.5, -15.2, -1.2)

<sup>a</sup>  $d(\text{Ir-O}_{1,2})=2.056 \text{ \AA}$ .

<sup>b</sup>  $d(\text{Ir-O}_1)=2.065 \text{ \AA}$ ,  $d(\text{Ir-O}_2)=2.083 \text{ \AA}$ .

The QC data in Table 1 indicate AF  $J$ 's, FM  $K$ 's and off-diagonal anisotropic couplings comparable in strength to the isotropic  $J$  interaction. Interestingly, the *ab initio* MRCI calculations indicate a much stronger  $K$  for nonorthogonal Ir-O-Ir bonds. This shows that deviations from rectangular geometry on the  $\text{Ir}_2\text{O}_2$  plaquette is *not* a negligible factor, as presently assumed in simplified superexchange models for Kitaev physics in honeycomb  $\text{Na}_2\text{IrO}_3$  [2, 13, 14]. The effect of the MRCI treatment is also stronger for nonorthogonal Ir-O-Ir bonds: the CAS+SOC  $K$  and  $D$  coupling parameters are enlarged by more than 50% by including O  $2p$  to Ir  $5d$  charge-transfer effects, Ir  $t_{2g}$  to  $e_g$  excitations and additional correlations accounted for in MRCI while  $J$  changes sign. This strong enhancement of the FM  $K$  for nonorthogonal Ir-O-Ir bonds and the tiny effect of the MRCI treatment on the FM  $K$  for rectangular geometry also disagrees with predictions of present approximate superexchange models that indicate the  $t_{2g}$  to  $e_g$  excitations and hopping as the dominant superexchange mechanism, giving rise to a large AF  $K$  [14].

Relative energies and the resulting effective coupling constants are next given in Table 2 for the experimentally determined  $C2/m$  crystal structure of Ref. [8]. For this set of calculations we used effective embedding potentials as described in Appendix A. There are two inequivalent Ir-Ir links in  $\text{Na}_2\text{IrO}_3$ , displaying different Ir-O-Ir bond angles and slightly different Ir-O and Ir-Ir distances [8]. While the  $[\text{Ir}_2\text{O}_{10}]$  block with larger Ir-O-Ir bond angles (upper part in Table 2) displays  $C_{2h}$  symmetry, for the other unit of edge-sharing octahedra the point-group symmetry is even further reduced to  $C_i$  (lower part in Table 2). The expressions of the spin-orbit wave functions in the transformed  $\{\tilde{S}_1, \tilde{S}_2, \tilde{M}_{S_1}, \tilde{M}_{S_2}\}$  basis show, however, that the mixing of the  $\Psi_i$  terms as expressed in

the idealized  $D_{2h}$  geometry is negligible in the  $C2/m$  structure. Therefore the *ab initio* data is mapped also in this case on the effective model described by (4).

As for the idealized  $D_{2h}$  configuration, the MRCI+SOC results indicate large FM Kitaev couplings, weaker AF Heisenberg superexchange and sizable  $D$  anisotropic interactions. The latter are not included in the plain KH model [2, 13, 14, 31] while the signs of  $K$  and  $J$  that we compute are different from those proposed in the recent model-Hamiltonian analysis of Ref. [14]. We note that in agreement with our findings, relatively large FM Kitaev couplings  $K$  have been earlier predicted by Kimchi and You [31] from the analysis of the phase diagram obtained by ED on modest size clusters and by Foyevtsova *et al.* [16] on the basis of an effective superexchange model fed with electronic-structure parameters obtained from density-functional calculations for the same  $C2/m$  structure [8]. However, the NN Heisenberg  $J$  is also FM in the latter work, different from the small AF values we find in the MRCI calculations. We also find that on each hexagonal  $\text{Ir}_6$  unit the two Ir-Ir links along the  $b$ -axis have effective coupling constants significantly different from the set of parameters associated with the other four Ir-Ir “bonds” due to subtly different oxygen distortions. Together these findings stress the importance of lattice distortions and symmetry issues and lay the foundation for rigorous *ab initio* investigations of unusually large anisotropic interactions such as the Kitaev exchange in strongly spin-orbit coupled  $5d$  oxides ‡.

It is known experimentally that  $\text{Na}_2\text{IrO}_3$  displays zigzag AF order at low  $T$ 's [8, 9, 24]. It has been also argued that the longer-range magnetic interactions, up to the second and third Ir coordination shells, are sizable and AF [8, 31, 35, 16]. We therefore performed ED calculations for a KH model supplemented with second and third NN couplings  $J_2$  and  $J_3$  (see Appendix B), on a 24-site cluster with periodic boundary conditions as used in earlier studies [13, 14]. We disregarded the presence of two structurally and magnetically different sets of Ir-Ir links and on the basis of the QC results of Table 2, used on all bonds  $J$ ,  $K$  and  $D$  coupling constants of 3,  $-17.5$  and  $-1$  meV, respectively (approximately averaged over all bonds). For a given set of  $J_2$  and  $J_3$  values the dominant order is determined according to the wave number  $\mathbf{Q} = \mathbf{Q}_{\max}$  giving a maximum value of the static structure factor  $S(\mathbf{Q})$ . The resulting phase diagram, see Fig. 2, shows that the zigzag phase is indeed stable in the region of  $J_2, J_3 \gtrsim 2$  meV. We note that positive  $J_2$  and  $J_3$  values of 4–5 meV would be consistent with the experimentally observed Curie-Weiss temperature  $\approx -125$  K [35] using  $\theta_{\text{CW}} = -\tilde{S}(\tilde{S} + 1)(J + 2J_2 + J_3 + K/3)/k_{\text{B}}$  [8]. Thus we propose that an extended spin Hamiltonian based on the nearest-neighbor anisotropic exchange terms found from the *ab initio* QC calculations supplemented by further-neighbor exchange integrals could provide a realistic starting point to explain the magnetism of  $\text{Na}_2\text{IrO}_3$ .

To discuss in more detail the generic phase diagram in Fig. 2, we note that in between the ordered phases we find a narrow spin liquid phase characterized by  $\mathbf{Q}_{\max} \simeq 0$

‡ Detailed QC studies of the anisotropic terms have been so far confined to  $3d$  oxides, where the spin-orbit interaction is just a small perturbation and the anisotropic coupling parameters are orders of magnitude weaker than the isotropic Heisenberg exchange [32, 33, 34].

and very weak spin-spin correlations. We checked that this phase is adiabatically connected to the Kitaev liquid phase appearing for larger  $|K|$  [13, 14]. The canted “stripe I” phase corresponds to the canted “phase III” found in earlier investigations of the isotropic  $J_1$ - $J_2$ - $J_3$  model [36, 37, 38]. Interestingly, a finite  $D$  enlarges the extent of both the spin liquid and the stripe I phases, showing that the planar spin fluctuations effectively amplify frustration in the model. The ED results show that the phase diagram is also very sensitive to the longer-range exchange couplings  $J_2$  and  $J_3$ . These findings are relevant in the context of recent experimental data that indicate a qualitatively different AF ground state for the related compound  $\text{Li}_2\text{IrO}_3$  [39].

### 3. Conclusions

In sum, for the honeycomb iridate  $\text{Na}_2\text{IrO}_3$ , the *ab initio* quantum chemistry calculations show that in a reference system with  $X$  along the Ir-Ir link and  $Z$  perpendicular on the  $\text{Ir}_2\text{O}_2$  plaquette the  $X$ - $Y$  anisotropy is significant and gives rise in the rotated  $(x, y, z)$  Kitaev-type frame [2, 13] to off-diagonal anisotropic terms beyond the plain Kitaev-Heisenberg model. Nevertheless, the calculations predict that the largest energy scale is the Kitaev interaction, 10 to 20 meV, while the NN Heisenberg superexchange and the off-diagonal  $xy$  coupling are significantly weaker. The quantum chemistry data additionally establish that the Kitaev term is FM. Further, all NN couplings are highly sensitive to subtle distortions involving the O ions. This makes the material dependence along the  $\text{Na}_2\text{IrO}_3$ ,  $\text{Li}_2\text{IrO}_3$  and  $\text{Li}_2\text{RhO}_3$  series an interesting topic for future

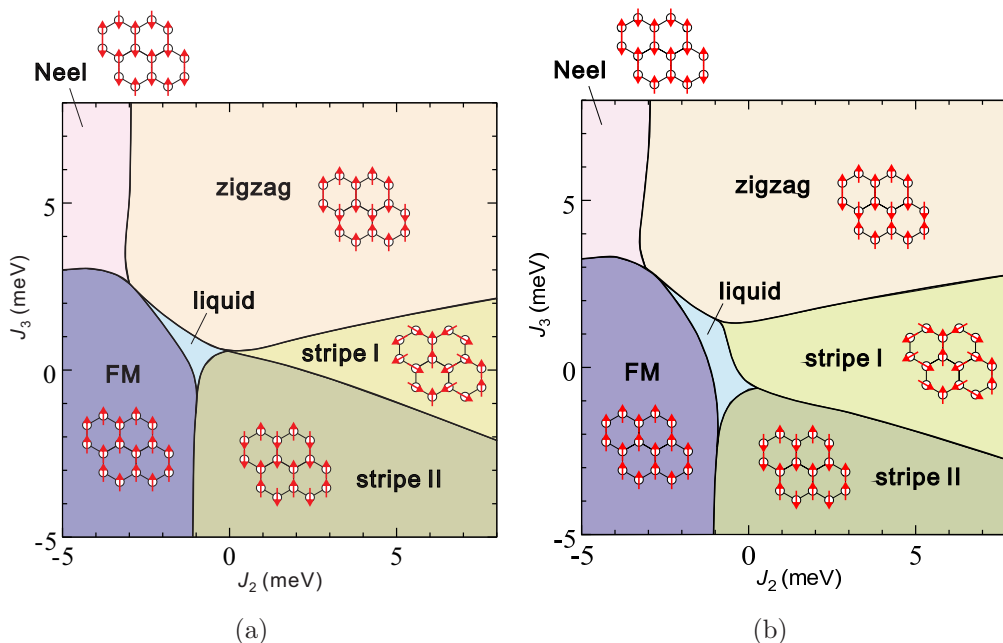


**Figure 2.** Phase diagram for the effective spin model in (4) supplemented by second and third NN couplings  $J_2$  and  $J_3$ , with  $J=3$  meV,  $K=-17.5$  meV and  $D=0$  (a) or  $D=-1$  meV (b), as found by exact diagonalizations on a 24-site cluster.



investigations. Large variations of the effective couplings as function of bond lengths and bond angles and a variable degree of “inequivalence” of those sets of parameters for structurally distinct Ir-Ir links in the honeycomb layer may in principle give rise to very different types of magnetic ground states in different  $5d^5$  or  $4d^5$  honeycomb compounds. Strong exchange anisotropy is also a topic of active research in the field of molecular magnetism and single-molecule magnets. The focus there has so far been on  $3d$  and  $4d$  compounds [40, 41, 42] but clearly  $5d$  systems with stronger spin-orbit couplings may provide new playgrounds in this research area too.

#### 4. Acknowledgements

We thank N. A. Bogdanov, G. Khaliullin, D. I. Khomskii, H. Gretarsson, Y.-J. Kim, H. Stoll and P. Fulde for insightful discussions. L. H. acknowledges financial support from the German Research Foundation (Deutsche Forschungsgemeinschaft, DFG).

#### 5. Appendix A: Computational details in the QC calculations

For the computation of the intersite spin couplings, two reference NN  $\text{IrO}_6$  octahedral units are considered. Since it is important to describe the finite charge distribution at sites in the immediate neighborhood [43, 44], the closest 22 Na neighbors and the other four, adjacent octahedra are also explicitly included in the actual cluster. However, to make the analysis of the low-lying magnetic states tractable, we cut off the spin couplings with the adjacent  $5d$  ions by replacing those open-shell  $\text{Ir}^{4+} 5d^5$  NN’s with closed-shell  $\text{Pt}^{4+} 5d^6$  species. This is an usual procedure in quantum chemistry studies on transition-metal systems, see, e.g., Refs. [45, 20, 21, 22, 23, 44, 46], and here allows a straightforward mapping of the *ab initio* data onto the effective spin model. It has been shown in earlier work that this way of modeling the NN  $5d$  ions does not affect the size of the  $t_{2g}$  splittings at the central, reference site [20, 21] and that the computed Heisenberg couplings agree well with estimates derived from experiment [20, 21]. The surrounding solid-state matrix is described as a finite array of point charges fitted to reproduce the crystal Madelung field in the cluster region. Most of the *ab initio* calculations were carried out with the MOLPRO quantum chemistry package [47]. Test calculations in finite magnetic fields were also performed with the ORCA program [48].

We used energy-consistent relativistic pseudopotentials with quadruple-zeta basis sets for the valence shells of the two reference Ir ions [49], all-electron quintuple-zeta basis sets for the bridging ligands [50] and triple-zeta basis functions for the other O’s of the two reference octahedra [50]. For the NN  $\text{Pt}^{4+} 5d^6$  species triple-zeta basis sets were applied [49] while the other O ions not shared with the central octahedra were modeled with minimal atomic-natural-orbital basis functions [51]. All occupied shells at the NN  $\text{Na}^+$  sites were incorporated in the large-core pseudopotentials and each of the Na  $3s$  orbitals was described with a single basis function [52]. For the central Ir ions and the two bridging ligands we also employed polarization functions, two Ir  $f$

and four  $d$  O functions [49, 50]. To separate the metal  $5d$  and O  $2p$  valence orbitals into different groups, we used the orbital localization module available in MOLPRO. The MRCI calculations were carried out for each spin multiplicity, singlet or triplet, as nine-root calculations. Only the four low-lying spin-orbit states are relevant for the analysis of the NN magnetic interactions. The higher-lying spin-orbit states imply an excitation energy of at least 0.6 eV. This gap concerns the  $j=1/2$  to  $j=3/2$  transitions [15].

The calculations in finite magnetic fields performed with the ORCA package were used to crosscheck the assignment of the lowest four magnetic states made on the basis of the dipole/quadrupole transition matrix elements, symmetry analysis and selection rules. These test calculations were carried out only for idealized  $D_{2h}$  structural models such as those of Table 1. It can be shown that when  $\mathbf{B} \parallel Oz$ ,  $\mathbf{B} \parallel Oy$  or  $\mathbf{B} \parallel Ox$ , state  $\Psi_1$ ,  $\Psi_2$  or  $\Psi_3$ , respectively, defined as in Table 1, should not change energy. This provides a quick alternative way of identifying the low-lying spin-orbit states.

## 6. Appendix B: Lattice spin model

In the main body of this article, we made use of two different local reference frames, namely  $\{\mathbf{x}_b, \mathbf{y}_b, \mathbf{z}_b\}$  and  $\{\mathbf{X}_b, \mathbf{Y}_b, \mathbf{Z}_b\} = \{\frac{\mathbf{x}_b + \mathbf{y}_b}{\sqrt{2}}, \frac{-\mathbf{x}_b + \mathbf{y}_b}{\sqrt{2}}, \mathbf{z}_b\}$ , for each of the three bond types  $b=1-3$ , see Fig. 3. Choosing the global frame to be  $\{\mathbf{x}, \mathbf{y}, \mathbf{z}\} \equiv \{\mathbf{x}_1, \mathbf{y}_1, \mathbf{z}_1\}$ , the local frames  $\{\mathbf{X}_b, \mathbf{Y}_b, \mathbf{Z}_b\}$  are expressed as

$$\begin{aligned} \{\mathbf{X}_1, \mathbf{Y}_1, \mathbf{Z}_1\} &= \left\{ \frac{\mathbf{x} + \mathbf{y}}{\sqrt{2}}, \frac{-\mathbf{x} + \mathbf{y}}{\sqrt{2}}, \mathbf{z} \right\}, \\ \{\mathbf{X}_2, \mathbf{Y}_2, \mathbf{Z}_2\} &= \left\{ \frac{\mathbf{x} - \mathbf{z}}{\sqrt{2}}, -\frac{\mathbf{x} + \mathbf{z}}{\sqrt{2}}, \mathbf{y} \right\}, \\ \{\mathbf{X}_3, \mathbf{Y}_3, \mathbf{Z}_3\} &= \left\{ \frac{\mathbf{y} + \mathbf{z}}{\sqrt{2}}, \frac{-\mathbf{y} + \mathbf{z}}{\sqrt{2}}, \mathbf{x} \right\}. \end{aligned} \quad (5)$$

We note that the system is invariant under a two-fold rotation around  $\mathbf{X}_1$  and that the directions of  $\mathbf{X}_2$  and  $\mathbf{X}_3$  are chosen to map to each other under this rotation (otherwise the sign of the exchange coupling parameter  $C$  is arbitrary).

To be explicit, let us write down all NN interaction terms for each of the three types of bonds  $b$  in the corresponding reference frame  $\{\mathbf{X}_b, \mathbf{Y}_b, \mathbf{Z}_b\}$ :

$$\begin{aligned} \mathcal{H}_{\langle ij \rangle \in b} &= J_{0,b} \tilde{\mathbf{S}}_i \cdot \tilde{\mathbf{S}}_j + A_b \tilde{S}_i^{X_b} \tilde{S}_j^{X_b} + B_b \tilde{S}_i^{Y_b} \tilde{S}_j^{Y_b} - (A_b + B_b) \tilde{S}_i^{Z_b} \tilde{S}_j^{Z_b} + C_b (\tilde{S}_i^{Y_b} \tilde{S}_j^{Z_b} + \tilde{S}_i^{Z_b} \tilde{S}_j^{Y_b}) \\ &= J_b \tilde{\mathbf{S}}_i \cdot \tilde{\mathbf{S}}_j + K_b \tilde{S}_i^{Z_b} \tilde{S}_j^{Z_b} + D_b (\tilde{S}_i^{X_b} \tilde{S}_j^{X_b} - \tilde{S}_i^{Y_b} \tilde{S}_j^{Y_b}) + C_b (\tilde{S}_i^{Y_b} \tilde{S}_j^{Z_b} + \tilde{S}_i^{Z_b} \tilde{S}_j^{Y_b}), \end{aligned} \quad (6)$$

where  $J_b = J_{0,b} + \frac{1}{2}(A_b + B_b)$ ,  $K_b = -\frac{3}{2}(A_b + B_b)$  and  $D_b = \frac{1}{2}(A_b - B_b)$ . We can rewrite these terms in the global frame  $\{\mathbf{x}, \mathbf{y}, \mathbf{z}\}$  using (5):

$$\begin{aligned} \mathcal{H}_{\langle ij \rangle \in b=1} &= J_1 \tilde{\mathbf{S}}_i \cdot \tilde{\mathbf{S}}_j + K_1 \tilde{S}_i^z \tilde{S}_j^z + D_1 (\tilde{S}_i^x \tilde{S}_j^y + \tilde{S}_i^y \tilde{S}_j^x) \\ &\quad + \frac{C_1}{\sqrt{2}} (\tilde{S}_i^y \tilde{S}_j^z + \tilde{S}_i^z \tilde{S}_j^y - \tilde{S}_i^x \tilde{S}_j^z - \tilde{S}_i^z \tilde{S}_j^x), \\ \mathcal{H}_{\langle ij \rangle \in b=2} &= J_2 \tilde{\mathbf{S}}_i \cdot \tilde{\mathbf{S}}_j + K_2 \tilde{S}_i^y \tilde{S}_j^y + D_2 (-\tilde{S}_i^x \tilde{S}_j^z - \tilde{S}_i^z \tilde{S}_j^x) \\ &\quad + \frac{C_2}{\sqrt{2}} (-\tilde{S}_i^x \tilde{S}_j^y - \tilde{S}_i^y \tilde{S}_j^x - \tilde{S}_i^z \tilde{S}_j^y - \tilde{S}_i^y \tilde{S}_j^z), \end{aligned}$$

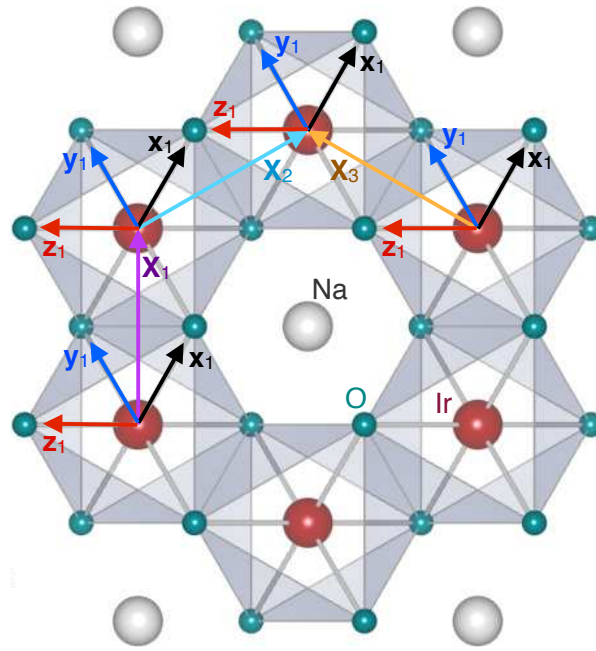


**Figure 3.** The two types of local reference frames,  $\{\mathbf{X}_b, \mathbf{Y}_b, \mathbf{Z}_b\}$  and  $\{\mathbf{x}_b, \mathbf{y}_b, \mathbf{z}_b\}$ , that are introduced for each of the three different types of bonds on the honeycomb layer.

$$\begin{aligned} \mathcal{H}_{\langle ij \rangle \in b=3} = & J_3 \tilde{\mathbf{S}}_i \cdot \tilde{\mathbf{S}}_j + K_3 \tilde{S}_i^x \tilde{S}_j^x + D_3 (\tilde{S}_i^y \tilde{S}_j^z + \tilde{S}_i^z \tilde{S}_j^y) \\ & + \frac{C_3}{\sqrt{2}} (-\tilde{S}_i^x \tilde{S}_j^y - \tilde{S}_i^y \tilde{S}_j^x + \tilde{S}_i^x \tilde{S}_j^z + \tilde{S}_i^z \tilde{S}_j^x). \end{aligned} \quad (7)$$

For  $\text{Na}_2\text{IrO}_3$  bonds 2 and 3 are equivalent and therefore  $J_2 = J_3$ ,  $K_2 = K_3$ ,  $D_2 = D_3$ ,  $C_2 = C_3$ .

In  $C_{2h}$  symmetry,  $D_b=0$  and for a given bond  $b$  the eigenvalues of the Hamiltonian defined by Eqn. 6 are

$$E_S = -\frac{3J_{0,b}}{4}, \quad (8a)$$

$$E'_1 = \frac{J_{0,b} + A_b + \sqrt{(A_b + 2B_b)^2 + 4C_b^2}}{4}, \quad (8b)$$

$$E'_2 = \frac{J_{0,b} + A_b - \sqrt{(A_b + 2B_b)^2 + 4C_b^2}}{4}, \quad (8c)$$

$$E_3 = \frac{J_{0,b} - 2A_b}{4}. \quad (8d)$$

These expressions become more complicated for point-group symmetries lower than  $C_{2h}$ . The analysis of the spin-orbit wavefunctions in the transformed  $\{\tilde{S}_1, \tilde{S}_2, \tilde{M}_{S_1}, \tilde{M}_{S_2}\}$  basis shows, however, that the mixing of the  $D_{2h}$   $\Psi_i$  eigenvectors for distorted clusters and lower symmetries of the  $[\text{Ir}_2\text{O}_{10}]$  blocks (see Table 2) is negligible in the  $C2/m$  structure determined by Choi *et al.* [8].

For  $D_{2h}$  symmetry (see Table 1),  $C_b = 0$  and the eigenvalues in the effective 2-site,

4-state problem are  $E_S = -3J_{0,b}/4$ ,  $E_1 = (J_{0,b} + 2A_b + 2B_b)/4$ ,  $E_2 = (J_{0,b} - 2B_b)/4$  and  $E_3 = (J_{0,b} - 2A_b)/4$ .

## References

- [1] Kitaev A 2006 *Ann. Phys.* **321** 2 – 111
- [2] Jackeli G and Khaliullin G 2009 *Phys. Rev. Lett.* **102** 017205
- [3] Baskaran G, Mandal S and Shankar R 2007 *Phys. Rev. Lett.* **98** 247201
- [4] Chen H D and Nussinov Z 2008 *J. Phys. A: Math. and Theor.* **41** 075001
- [5] Vidal J, Schmidt K P and Dusuel S 2008 *Phys. Rev. B* **78** 245121
- [6] Tikhonov K S, Feigel'man M V and Kitaev A Y 2011 *Phys. Rev. Lett.* **106** 067203
- [7] Nussinov Z and van den Brink J *arXiv:1303.5922 (unpublished)*
- [8] Choi S K, Coldea R, Kolmogorov A N, Lancaster T, Mazin I I, Blundell S J, Radaelli P G, Singh Y, Gegenwart P, Choi K R, Cheong S W, Baker P J, Stock C and Taylor J 2012 *Phys. Rev. Lett.* **108** 127204
- [9] Ye F, Chi S, Cao H, Chakoumakos B C, Fernandez-Baca J A, Custelcean R, Qi T F, Korneta O B and Cao G 2012 *Phys. Rev. B* **85** 180403
- [10] Thornley J H M 1968 *J. Phys. C (Proc. Phys. Soc.)* **1** 1024
- [11] Abragam A and Bleaney B 1970 *Electron Paramagnetic Resonance of Transition Ions* (Clarendon Press, Oxford)
- [12] Kim B J, Jin H, Moon S J, Kim J Y, Park B G, Leem C S, Yu J, Noh T W, Kim C, Oh S J, Park J H, Durairaj V, Cao G and Rotenberg E 2008 *Phys. Rev. Lett.* **101** 076402
- [13] Chaloupka J, Jackeli G and Khaliullin G 2010 *Phys. Rev. Lett.* **105** 027204
- [14] Chaloupka J, Jackeli G and Khaliullin G 2013 *Phys. Rev. Lett.* **110** 097204
- [15] Gretarsson H, Clancy J P, Liu X, Hill J P, Bozin E, Singh Y, Manni S, Gegenwart P, Kim J, Said A H, Casa D, Gog T, Upton M H, Kim H S, Yu J, Katukuri V M, Hozoi L, van den Brink J and Kim Y J 2013 *Phys. Rev. Lett.* **110** 076402
- [16] Foyevtsova K, Jeschke H O, Mazin I I, Khomskii D I and Valentí R 2013 *Phys. Rev. B* **88** 035107
- [17] Yushankhai V and Hayn R 1999 *Europhys. Lett.* **47** 116
- [18] Tornow S, Entin-Wohlman O and Aharony A 1999 *Phys. Rev. B* **60** 10206
- [19] Liu X, Katukuri V M, Hozoi L, Yin W G, Dean M P M, Upton M H, Kim J, Casa D, Said A, Gog T, Qi T F, Cao G, Tsvelik A M, van den Brink J and Hill J P 2012 *Phys. Rev. Lett.* **109** 157401
- [20] Katukuri V M, Stoll H, van den Brink J and Hozoi L 2012 *Phys. Rev. B* **85** 220402
- [21] Bogdanov N A, Katukuri V M, Stoll H, van den Brink J and Hozoi L 2012 *Phys. Rev. B* **85** 235147
- [22] Hozoi L, Gretarsson H, Clancy J P, Jeon B G, Lee B, Kim K H, Yushankhai V, Fulde P, Y-J Kim and van den Brink J *arXiv:1212.4009 (unpublished)*.
- [23] Bogdanov N A, Maurice R, Rousochatzakis I, van den Brink J and Hozoi L 2013 *Phys. Rev. Lett.* **110** 127206
- [24] Liu X, Berlijn T, Yin W G, Ku W, Tsvelik A, Kim Y J, Gretarsson H, Singh Y, Gegenwart P and Hill J P 2011 *Phys. Rev. B* **83** 220403
- [25] Gretarsson H, Clancy J P, Singh Y, Gegenwart P, Hill J P, Kim J, Upton M H, Said A H, Casa D, Gog T and Kim Y J 2013 *Phys. Rev. B* **87** 220407
- [26] Helgaker T, Jørgensen P and Olsen J 2000 *Molecular Electronic-Structure Theory* (Wiley, Chichester)
- [27] Fink K, Fink R and Staemmler V 1994 *Inorg. Chem.* **33** 6219
- [28] van Oosten A B, Broer R and Nieuwpoort W C 1996 *Chem. Phys. Lett.* **257** 207
- [29] Broer R, Hozoi L and Nieuwpoort W C 2003 *Mol. Phys.* **101** 233
- [30] Calzado C J, Evangelisti S and Maynau D 2003 *J. Phys. Chem. A* **107** 7581
- [31] Kimchi I and You Y Z 2011 *Phys. Rev. B* **84** 180407
- [32] Maurice R, Pradipto A M, Guihéry N, Broer R and de Graaf C 2010 *J. Chem. Theo. Comput.* **6** 3092–3101

- [33] Pradipto A M, Maurice R, Guihéry N, de Graaf C and Broer R 2012 *Phys. Rev. B* **85** 014409
- [34] Maurice R, Pradipto A M, de Graaf C and Broer R 2012 *Phys. Rev. B* **86** 024411
- [35] Singh Y, Manni S, Reuther J, Berlijn T, Thomale R, Ku W, Trebst S and Gegenwart P 2012 *Phys. Rev. Lett.* **108** 127203
- [36] Rastelli E, Tassi A and Reatto L 1979 *Physica B+C* **97** 1
- [37] Fouet J B, Sindzingre P and Lhuillier C 2001 *Eur. Phys. J. B* **20** 241
- [38] Albuquerque A F, Schwandt D, Hetényi B, Capponi S, Mambrini M and Läuchli A M 2011 *Phys. Rev. B* **84** 024406
- [39] Cao G, Qi T F, Li L, Terzic J, Yuan S J, Tovar M, Murthy G and Kaul R K *arXiv:1307.2212* (unpublished)
- [40] Mironov V S, Chibotaru L F and Ceulemans A 2003 *J. Am. Chem. Soc.* **125** 9750
- [41] Maurice R, Guihéry N, Bastardis R and de Graaf C 2010 *J. Chem. Theory Comput.* **6** 55
- [42] Palić A, Tsukerblat B, Klokishner S, Dunbar K R, Clemente-Juan J M and Coronado E 2011 *Chem. Soc. Rev.* **40** 3130
- [43] Hozoi L, Siurakshina L, Fulde P and van den Brink J 2011 *Sci. Rep.* **1** 65
- [44] de Graaf C, Sousa C and Broer R 1999 *J. Mol. Struct. (Theochem)* **458** 53
- [45] Hozoi L, de Vries A H, van Oosten A B, Broer R, Cabrero J and de Graaf C 2002 *Phys. Rev. Lett.* **89** 076407
- [46] Maurice R, Verma P, Zadrozny J M, Luo S, Borycz J, Long J R, Truhlar D G and Gagliardi L 2013 *Inorg. Chem.* **52** 9379
- [47] Werner H J, Knowles P J, Knizia G, Manby F R and Schütz M MOLPRO 2012, University of Cardiff, see <http://www.molpro.net>
- [48] Neese F 2012 *WIREs: Comput. Mol. Sci.* **2** 73–78
- [49] Figgen D, Peterson K A, Dolg M and Stoll H 2009 *J. Chem. Phys.* **130** 164108
- [50] Dunning T H 1989 *J. Chem. Phys.* **90** 1007–1023
- [51] Pierloot K, Dumez B, Widmark P O and Roos B 1995 *Theor. Chim. Acta* **90** 87–114
- [52] Fuentealba P, Preuss H, Stoll H and von Szentpály L 1982 *Chem. Phys. Lett.* **89** 418